Metastable conduction states in Mo_2S_3: Pulse conductivity and thermoelectric power

R. L. Fagerquist* and Roger D. Kirby
Behlen Laboratory of Physics, University of Nebraska–Lincoln, Lincoln, Nebraska 68588-0111
(Received 31 December 1987)

Mo_2S_3 is a linear-chain-structure compound which has two inequivalent zig-zag Mo chains parallel to the *b* axis. It undergoes at least two phase transitions below room temperature (at 182 and 145 K upon cooling). X-ray-diffraction measurements show that both incommensurate and commensurate structural distortions are associated with the phase transitions. We report here the results of electrical-conductivity and thermoelectric-power measurements on Mo_2S_3. By using pulsed electric currents to rapidly heat and cool the sample while electrical-resistivity or thermoelectric-power measurements are being made, we are able to show that below the lower-temperature phase transition, the carriers in Mo_2S_3 can be either in a poorly conducting ground state or in a relatively highly conducting metastable state. The lifetime of a carrier in the metastable state is strongly dependent on the temperature and is more than 200 s at 77 K. The temperature dependence of the conductivity and all of the pulse conductivity measurements are consistent with a phenomenological double-well-potential model for the carrier in Mo_2S_3. Three possible models which can give rise to such a double-well potential are discussed: (1) a defect-trapping model, (2) an acoustic-polaron model, and (3) a charge-density-wave model.

I. INTRODUCTION

In its single-crystal form, Mo_2S_3 exists as long, needlelike fibers which have a metallic luster. In external appearance, it resembles the quasi-one-dimensional conductors $NbSe_3$ and TaS_3. These latter compounds have extremely anisotropic physical properties and, further, they undergo charge-density-wave–induced phase transitions to structurally distorted states at low temperatures. As a result of this, they show a number of unusual electrical-transport properties, including nonlinear conduction and large frequency-dependent fluctuations in the electrical conductivity.[1–6] X-ray-diffraction and transport-property measurements show that Mo_2S_3 also undergoes phase transitions to structurally distorted states at low temperatures[7–13] and so one might anticipate that it would also exhibit some unusual conductivity properties. It will be seen later that this is indeed the case, but that the conduction properties of Mo_2S_3 are quite different from those observed in $NbSe_3$ and TaS_3 and, further, that the explanation of these properties will require a physical model very different from those used to describe $NbSe_3$ and TaS_3.

Jellinek[7] first determined the average room-temperature crystal structure of the powder form of Mo_2S_3 and found it to be monoclinic with the following unit-cell parameters: $a=6.092$ Å, $b=3.208$ Å, $c=8.633$ Å, and $\beta=102.43°$. This structure was also found by Kadjik *et al.*[8] The x-ray measurements of DeJonge *et al.*[9] showed that the crystal structure becomes triclinic below 173 K, and their transport measurements showed that a first-order phase transition took place at this temperature. This transition was found to have a large hysteresis, occurring at about 190 K upon warming. Thermoelectric-power,[9,10] and Hall[10] measurements showed that the primary charge carriers are holes, with a concentration in the range of 10^{20}–$10^{21}/cm^3$.

Rashid *et al.*[12] carried out temperature-dependent electrical-resistivity, magnetic-susceptibility, and Raman-scattering measurements on Mo_2S_3 between 4 and 300 K. Their results show that there are two first-order phase transitions below 300 K (at 182 and 145 K upon cooling) and, in addition, they observed an anomalous peak in the resistivity at about 80 K. They found that this peak decreased substantially in magnitude if the cooling rate was increased above 1 K/min. Rastogi[13] studied this effect in more detail and noted that if the sample were quenched to a temperature near 140 K the resistivity showed a logarithmic dependence on time, indicating that the lower-temperature phase transition is very sluggish. Deblieck *et al.*[11] carried out x-ray-diffraction measurements between 100 and 400 K and found structural distortions both commensurate and incommensurate with the lattice below room temperature.

More recently, Alova and Mozurkewich[14] investigated the elastic properties of Mo_2S_3 below room temperature using the vibrating-reed technique. They found a large peak in the internal friction at temperatures between 130 and 150 K for frequencies between 2 and 33 kHz. The temperature and frequency dependencies of this peak indicate that it is due to a thermally activated process.

Rashid *et al.*[12] suggested that the phase transitions in Mo_2S_3 could be due to the formation of charge-density waves at the phase-transition temperatures, such as has been observed in a number of the transition-metal dichalcogenides ($NbSe_2$, $TiSe_2$, and TaS_2) (Refs. 15–18) and trichalcogenides ($NbSe_3$, TaS_3, and NbS_3).[1–6] As a consequence of charge-density-wave formation, the trichalcogenides, in particular, often exhibit interesting transport phenomena, including such effects as nonlinear con-

ductivity, excess broadband electrical noise, coherent narrow-band noise, and anomalous ac conductivity.[19–23] These phenomena appear to be direct consequences of the collective nature of the charge carriers which have been "frozen out" in the charge-density wave. This type of collective behavior was first hinted at by the theoretical work of Peierls[24] and Fröhlich[25] on one-dimensional conductors.

Since Mo_2S_3 exhibits phase transitions which are accompanied by a loss of Fermi surface, and since it has the outward appearance of a quasi-one-dimensional conductor, we made a more detailed study of its low-temperature transport properties. It was expected that phenomena similar to those observed in the transition-metal trichalcogenides would be found. Instead, a completely different kind of conductivity behavior was observed. In the experiments to be discussed here, a current pulse was used to Joule-heat the sample a few K, and the sample conductivity was measured as a function of time after removal of the pulse. These measurements show that below the lower-temperature phase transition (about 145 K upon cooling) a long-lived metastable electronic conducting state coexists with a lower-conductivity electronic ground state. The lifetime of a carrier in the metastable state was found to depend exponentially on the temperature and to be about 200 s at 77 K. The existence of the metastable conduction state results in an unusual time-dependent conductivity behavior. It will be seen that for $T<145$ K both the temperature-dependent conductivity and the time-dependent conductivity are consistent with a phenomenological double-well-potential model for the charge carriers.

II. CRYSTAL STRUCTURE AND TRANSPORT PROPERTIES

A. Crystal structure

Deblieck *et al.*[11] recently determined the crystal structure of $Mo_{2.065}S_3$ as a function of temperature. At room temperature they found the average structure to be monoclinic [space group $P2_1/m$ (C_{2h}^2)] with 10 atoms per unit cell, as shown in Fig. 1. The Mo atoms are arranged in two inequivalent zig-zag chains along the crystalline b axis, with type-1 chains lying nearly in the (101) plane and type-2 chains lying nearly in the (001) plane. The actual room-temperature structure of $Mo_{2.065}S_3$ is more complex than this, with small incommensurate distortions of wave vectors $(p, \frac{1}{2}, q)$ and $(\frac{1}{2}, \frac{1}{2}-v, 0)$ existing, with $p=-0.041$, $q=0.214$, and $v=0.059$. Deblieck *et al.* found that the distortion wave vectors varied with temperature according to

$$\mathbf{k}_1:\ (0,\tfrac{1}{2},0)\xrightarrow{\sim 110\ \mathrm{K}}(0,\tfrac{1}{2},\tfrac{1}{4})\xrightarrow{\sim 200\ \mathrm{K}}(p,\tfrac{1}{2},q)\ ,$$

$$\mathbf{k}_2:\ (\tfrac{1}{2},\tfrac{1}{2},0)\xrightarrow{\sim 150\ \mathrm{K}}(\tfrac{1}{2},\tfrac{1}{2},0.153)\xrightarrow{180\ \mathrm{K}}(\tfrac{1}{2},\tfrac{1}{2}-v,0)\ ,$$

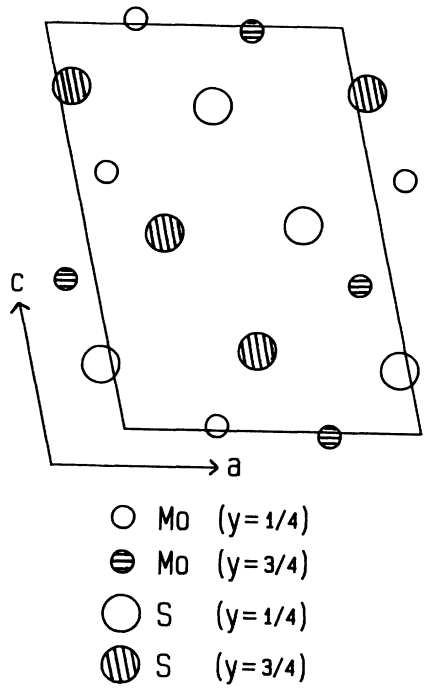

FIG. 1. Average crystal structure of Mo_2S_3 at room temperature. There are two inequivalent types of Mo-Mo chains parallel to the crystalline b axis. The crystal structure is monoclinic [space group $P2_1/m$ (C_{2h}^2)], with lattice parameters $a=8.633$ Å, $b=3.208$ Å, $c=6.092$ Å, and $\beta=102.43°$.

with the distortion wave vectors $\mathbf{k}_1$ and $\mathbf{k}_2$ associated with distortions in the type-1 and -2 chains, respectively. Below 180 K the Mo atoms cluster together in four-atom units, apparently because of the strong metal-metal bonding. Further, Deblieck *et al.* observed some crystals to be multidomained, with two variants differing by a rotation of 102.4° about the b axis. $\mathbf{k}_1$ and $\mathbf{k}_2$ showed somewhat different temperature dependencies in the multidomain crystals.

B. Crystal growth and analysis

Single-crystal samples of Mo_2S_3 were grown using the vapor-phase–transport method with iodine as the transporting agent. Stoichiometric proportions of molybdenum and sulfur powders were sealed in evacuated quartz tubes with an iodine charge of 5 mg/cm^3 of tube volume. The tubes were placed in a three-zone furnace, with the starting-materials end of the tube at 1100 °C and the growth end at 1025 °C. After a 2-week growth period the furnace was turned off and allowed to cool slowly. Single crystals of Mo_2S_3 (typical dimensions $20\times 50\times 5000$ μm^3) were found in the growth end of the tube.

Chemical analysis of the crystals revealed the composition to be $Mo_2S_{3.2\pm 0.2}$. A slightly-metal-rich composition, as has been found by others,[26,27] cannot be ruled out. X-ray-diffraction measurements at room temperature using a standard 57.3-mm powder camera with a Gandolfi attachment revealed 20 diffraction lines which could be indexed using the lattice parameters reported by

Jellinek.[7] No iodine above the detection limit of 2 at. % was observed in x-ray-fluorescence measurements.

C. Temperature-dependent resistivity of Mo_2S_3

The single-crystal samples of Mo_2S_3 were mounted on specially designed printed-circuit boards such that the resistivity along the *b* axis (the longest crystal dimension) was measured. The samples were attached to copper fingers on the circuit board using silver paint in a standard four-probe configuration, with the two outer contacts being connected to a constant-current source and the two inner contacts being used for the sample voltage measurement. The mounted sample was inserted inside a copper can in the resistivity cryostat, and the temperature of the can was controlled by means of a resistance heater wound around its outside. The sample temperature was measured using calibrated-silicon-diode or platinum-resistance thermometers.

Figure 2 shows the electrical resistivity of Mo_2S_3 as a function of temperature. These results show several unusual features, as have been reported earlier.[12] Upon cooling from room temperature, the resistivity falls smoothly, until it undergoes a sharp increase near 180 K. A second increase is observed at 145 K, and a large peak in the resistivity is found at 80 K. Upon warming from low temperatures, sharp decreases in the resistivity are noted at 175 and 192 K, suggesting that both phase transitions are first order. The warming curve finally joins up with the cooling curve at 285 K. The temperatures of the phase transitions show perhaps a ±3-K sample-to-sample variation. The resistivity measurements of Rashid *et al.*[12] and of Rastogi[13] show that the size of the 80-K resistivity peak is dramatically reduced for sample cooling rates greater than about 1 K/min. In particular, the rise in resistivity below 145 K is quite sluggish, with small increases in the resistivity occurring (while the temperature is held constant) over periods of hours. Rastogi[13] has studied this effect in some detail. Identical resistivity curves were obtained for samples with pressed copper contacts instead of silver paint. Further, no aging effects were observed over periods of many months. The magnitude of the resistivity at room temperature was typically 1.5×10^{-3} Ω cm.

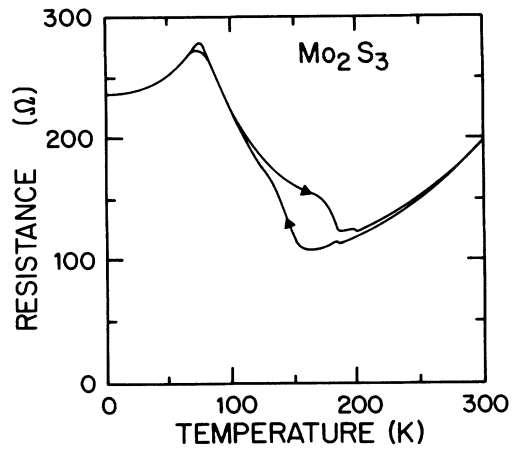

FIG. 2. Electrical resistivity of Mo_2S_3 along the crystalline *b* axis.

D. Thermoelectric-power measurements

A schematic diagram of the thermoelectric-power sample holder is shown in Fig. 3. The ends of the sample were clamped to copper blocks A and B, using copper clamps. Blocks A and B each have resistance heaters attached, so that their temperatures can be controlled independently. The temperature difference between blocks A and B and, hence, of the two ends of the sample, was monitored with a copper-constantan thermocouple. The two junctions of the thermocouple are in thermal, but not electrical, contact with blocks A and B. Copper wires running from blocks A and B to the top of the cryostat were used to measure the sample thermoelectric power. A Keithley model 158 nanovoltmeter was used for this purpose. In order to maintain a uniform sample temperature, the whole sample mount fits inside a copper cylinder, which is heated by means of a resistance heater.

Two different methods were used to measure the thermoelectric power of Mo_2S_3. In the first method the temperature of the sample mount was monitored with the platinum thermometer and controlled using a computer-based temperature controller. Copper block A was heated using the voltage from a low-frequency (typically 0.001 Hz) ramp generator. The copper-constantan reference thermocouple was monitored using a Keithley nanovoltmeter and its output was sent to the *x*-axis input of an *x-y* recorder. Simultaneously, the sample thermopower was monitored by a second Keithley nanovoltmeter, and its output was sent to the *y*-axis input of the *x-y* recorder. As the ramp voltage increased, the temperature difference between the two copper blocks increased, and the *x-y* recorder traced out a straight line. The slope of this straight line is proportional to the thermoelectric power of Mo_2S_3 relative to copper. The advantage of this method is that the effects of stray thermal electromotive forces (emf's) are largely eliminated, since only the slope dV_T/dT is measured. It is, however, a very slow measurement method since the sample mount must attain thermal equilibrium at the desired temperature before the thermoelectric power can be measured.

The second method used allowed thermoelectric-power data to be acquired much more rapidly. In this method the platinum thermometer was read using a digital voltmeter interfaced to a Digital Equipment Corporation LSI-11 computer. The computer converted the thermometer reading to a temperature, and slowly scanned the temperature up or down by means of an analog-to-digital converter and a resistance heater wound around the sample-mount enclosure. The same computer was used to read the reference thermocouple voltage and the sample thermal emf (after amplification by Keithley nanovoltmeters), and also to control the temperature difference between the two ends of the sample. The computer determined the base temperature from the platinum-thermometer reading, and then calculated the desired voltage from the reference thermocouple. It then

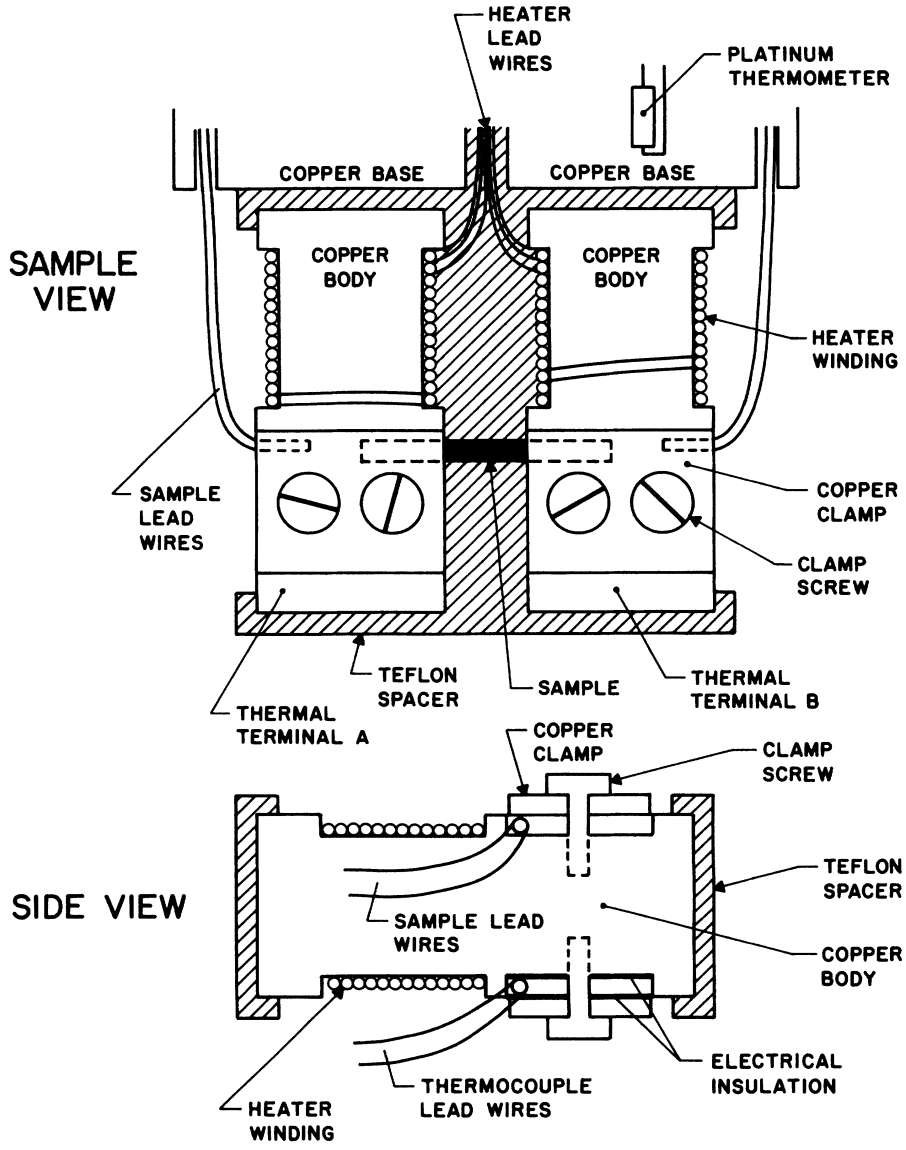

FIG. 3. Expanded view of the thermoelectric-power sample-holder assembly.

controlled the temperature difference between the two ends of the sample (usually 0.5–1.0 K) by adjusting the current through the heater on block A. The computer averaged the sample thermal emf until the base temperature had changed a present amount (typically 0.25–0.5 K), when it would record the thermoelectric power on a floppy diskette. Stray thermal emf's appeared to be less than 1 μV.

Figure 4 shows the thermoelectric power of Mo_2S_3 as a function of temperature using the second (computer-based) method. Thermopower data taken on other samples using the first method agree with these measurements to within ± 2 μV/K. The thermoelectric power of a given sample also reproduces upon temperature cycling to within these limits. (Although we did not study the dependence of the thermoelectric power cooling rate, it seems likely that it will show behavior similar to that observed in the resistivity.[12,13]) One should first note that the thermoelectric power is positive, indicating that the primary carriers are holes. As the temperature is lowered from 300 K, the thermoelectric power falls slowly from 64 μV/K, with a small, sharp drop at 283 K. At about 180 K the thermoelectric power rises, indicating the occurrence of the first phase transition. As the temperature is lowered further, the thermoelectric power increases smoothly. The second phase transition is not as well defined as it was in the resistivity data shown earlier and in the magnetic-susceptibility measurements of Rashid *et al.*[12] Upon warming, the thermopower shows hysteresis similar to that observed in the resistivity measurements. Note that the drop in thermopower associated with the lower-temperature phase transition is quite sharp.

Figure 5 shows the measured temperature derivatives of the thermoelectric power for both cooling and warming for the Mo_2S_3 sample. Figure 5(a) shows the tempera-

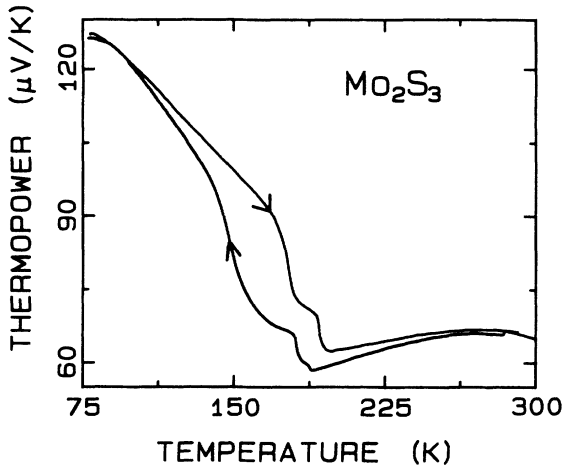

FIG. 4. Thermoelectric power of Mo_2S_3 relative to copper as a function of temperature for both heating and cooling, as indicated by the arrows. These measurements were taken using the scanning-temperature technique.

ture derivative upon cooling from room temperature. A peak in the derivative is clearly evident at 283 K in the cooling curve, indicating the presence of the anomaly observed in the resistivity. The curve clearly shows the phase transitions at 180 and 145 K. The small dip near 185 K is not reproducible. Figure 5(b) shows that the two phase transitions occur at 175 and 192 K upon warming from low temperatures. There is perhaps a weak negative peak at 287 K, corresponding to the temperature where the warming curve recombines with the cooling curve.

III. NONEQUILIBRIUM TRANSPORT IN Mo_2S_3

A. Nonequilibrium electrical conductivity

We carried out a series of conductivity measurements using pulsed currents which show that the carriers in

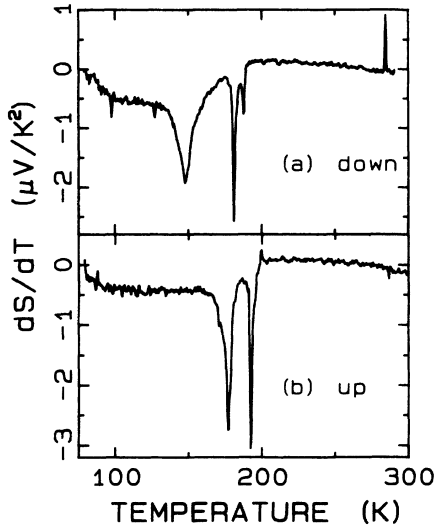

FIG. 5. Temperature derivative of the thermoelectric power for Mo_2S_3. (a) Upon cooling from room temperature. (b) Upon warming from low temperature.

Mo_2S_3 can exist in metastable conduction states. A schematic representation of the experimental procedure and the results obtained is shown in Fig. 6. Figure 6(a) shows the current through the sample as a function of time. Initially, a large dc current (typically a few mA) is passed through the sample. This current is large enough to Joule-heat the sample a few K, as is indicated in Fig. 6(b). After the sample has approached equilibrium at this elevated temperature, the current is reduced by an order of magnitude or more, so that the sample cools rapidly to near its original temperature. As will be seen, the time constant for heating or cooling the sample appears to be typically 1 ms. Figure 6(c) shows schematically the observed conductivity as a function of time during this procedure. At the onset of the large current pulse, the sample conductivity falls rapidly for the first few ms, goes through a minimum, and then approaches approximately exponentially a fixed value from below. When the current is lowered, the conductivity first rises rapidly, goes through a maximum, and then falls exponentially with a very long time constant which depends on the temperature.

To carry out these measurements, the sample was mounted in the four-probe configuration discussed earlier, and the measurements were obtained using the LSI-11 computer in conjunction with digital-to-analog and analog-to-digital converters. One digital-to-analog converter was used to supply the current pulse to the sample. The sample voltage was then amplified using an Ithaco model 1201 amplifier and measured at equally spaced

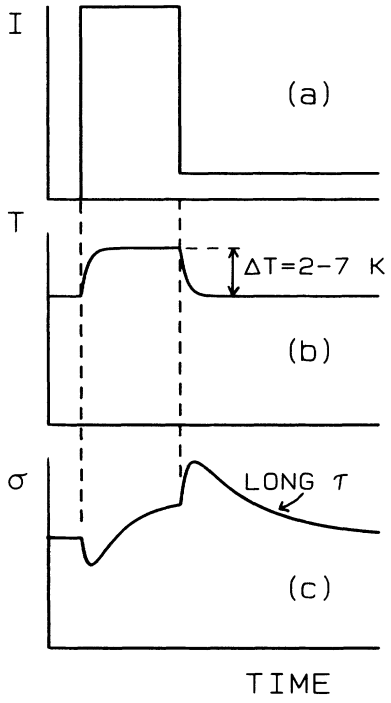

FIG. 6. Schematic behavior of the conductivity of Mo_2S_3 during a pulsed-current–conductivity measurement. (a) Sample current vs time. (b) Sample temperature vs time. (c) Sample conductivity vs time.

time intervals using a 12-bit analog-to-digital converter. The rate of measurement of the sample voltage was varied from 0.1 Hz to 10 kHz, depending on the time scale desired. During this time, the computer was also used to read the thermometer and control the sample temperature.

A typical plot of the conductance of Mo_2S_3 as a function of time is shown in Fig. 7 for a sample temperature of 100 K. The data appearing on the left-hand side of the figure (above the axis labeled t_H) is the sample conductance as a function of time, $G(t)$, during the high-current pulse. The right-hand side of this plot, above the t_L axis, shows the sample conductance for times after the onset of the lower current. The origin of each plot is indicated by t_H or $t_L=0$. It should be noted that the time scales for the two sets of data are quite different.

In the high-current–pulse data a sharp minimum occurs in $G(t)$ near $t_H=0$. The horizontal dashed line in Fig. 7 shows the value of the low-current conductivity. Immediately after the minimum, $G(t)$ increases with time until it reaches an almost constant value. This relatively large increase in $G(t)$ is due to the increased sample conductivity at the elevated temperature. (The conductivity of Mo_2S_3 increases with increasing temperature in this temperature region.) The rise in sample temperature during the high-current pulse was estimated from the magnitude of the change of the sample conductivity. The current during the high-current pulse was set at a value such that the increase in sample temperature was between 2 and 7 K. The much slower increase in $G(t)$ that follows this is likely due to the slow heating of the sample contacts and the surrounding exchange gas, the details of which are unimportant for this experiment. The more interesting occurrence of the minimum near $t_H=0$ cannot, however, be explained by a simple heating effect, and it will be discussed later.

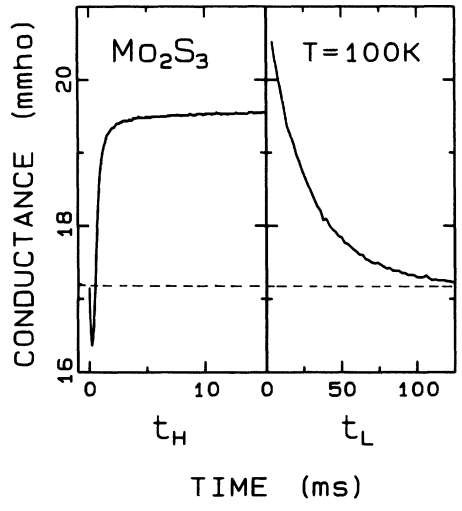

FIG. 7. Electrical conductivity of Mo_2S_3 as a function of time at $T=100$ K. The left-hand side of the graph is the conductivity during the large current pulse, while the right-hand side of the graph is the conductivity after the onset of the lower current. Note the different time scales during the low- and high-current measurements.

After $t_L=0$ (the onset of the lower current), the first measured data point shows that the sample conductance is larger than that given by the last high-current–pulse data point. (Data taken at more rapid sampling rates show that the conductance immediately after $t_L=0$ rises from the high-current value and goes through a maximum similar to the initial minimum during the high-current pulse.) The conductance then decreases with time, asymptotically approaching the value of the conductance of the sample before the application of the current pulse.

Let us now concentrate on the sample conductivity after the onset of the lower current. Figure 8 shows the measured time dependence of the sample conductivity after the onset of the lower current for three different sample temperatures. The experimental data points are shown as points, while the solid lines are nonlinear least-squares fits to the equation

$$G(t_L)=G_0+\Delta G_0 \exp(-t_L/\tau) , \quad (1)$$

where G_0 is the low-current value of the conductance at

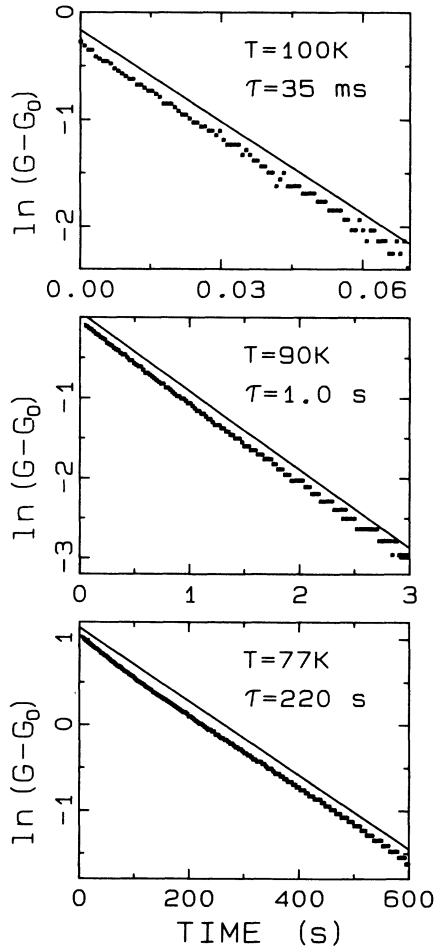

FIG. 8. Electrical conductivity of Mo_2S_3 during the low-current pulse for three different temperatures. The points are the measured conductivities, while the solid curves are least-squares fits to Eq. (1). The fitted curves have been displaced vertically for clarity.

$t_L=\infty$, and $\Delta G_0=G(t_L=0)-G(t_H=0)$. The constant τ is the characteristic relaxation time for the conductivity at the temperature of the measurement. Note that Fig. 8 actually shows $\ln[G(t_L)-G(\infty)]$ as a function of time, and that the fitted curves have been displaced upwards a small amount for clarity.

The good fits of Eq. (1) to the data for the three temperatures of Fig. 8 indicate that the time dependence observed for the sample conductance after the onset of the lower current can be represented by an exponential function of time, characterized by a single relaxation-time constant τ. Furthermore, τ is strongly temperature dependent, varying from a few ms to a few hundred seconds as the temperature is changed from 105 to 77 K. Several points should be made about these observations. First, the complicated time-dependent conductance, shown in Figs. 6 and 7, cannot be explained by a simple heating effect. During either the high-current pulse or after the onset of the lower current, the conductance both increases and decreases. Second, the observed relaxation times, at least at low temperatures, seem far too large to be ascribed to time constants associated heating or cooling of the sample. As the temperature is raised above 110 K, the time constant measured in this fashion saturates at approximately 1 ms, depending on sample size. This time constant appears to be roughly the right magnitude to be a heating or cooling time constant.

The temperature dependence of τ is shown explicitly in Fig. 9, where $\log_{10}(\tau)$ is plotted as a function of $1/T$. The squares are the values of τ obtained from the measurements, while the solid line is a least-squares fit to the equation

$$\tau=\tau_0\exp(W/kT)\ . \tag{2}$$

The parameters τ_0 and W are determined from the fit, and k is Boltzmann's constant. The data shown in this figure were taken on a single Mo_2S_3 sample, and they correspond to $W=0.256$ eV and $\tau_0=5.1\times10^{-15}$ s. Measurements on a number of different samples resulted in nearly identical values of W ($0.25<W<0.26$ eV), and τ_0 between 10^{-14} and 10^{-15} s. The somewhat large variation in τ_0 is not unexpected, since τ_0 is determined by an extrapolation to $T=\infty$.

It should be noted that identical results are obtained for samples with pressed-copper contacts, rather than silver-paint contacts. Also, the time-constant effects are observed in samples heated with an argon laser beam rather than with a current pulse.

The internal-friction measurements carried out by Alova and Mozurkewich[14] show that the internal-friction peak is caused by a thermal-activation process. Their values for W and τ_0 were found to be 0.33 ± 0.03 eV and $\sim10^{-16}$ s, respectively. These values, while not identical to the values obtained here, do suggest that the internal-friction peak arises from the same physical origins as the nonequilibrium conductivity.

B. Nonequilibrium thermoelectric power

Time-constant effects similar to those described above are also observed in the thermoelectric power of Mo_2S_3. The sample was mounted in the thermoelectric-power cryostat and a temperature gradient was set up across the sample. The sample was then heated a few K with a current pulse. After removal of the current pulse, the sample voltage (the thermal emf) was measured as a function of time. Since a Keithley nanovoltmeter was used to measure the thermal emf, these measurements were limited to the low-temperature range, where the time constant is rather long. Figure 10 shows the thermal emf as a function of time for a sample temperature of 77 K (pluses). For comparison, the resistance as a function of time measured on the same sample (at a different time, but with the same temperature gradient present) is also shown (squares). (During the resistance measurements, the sample voltage due to the iR drop was 3 orders of

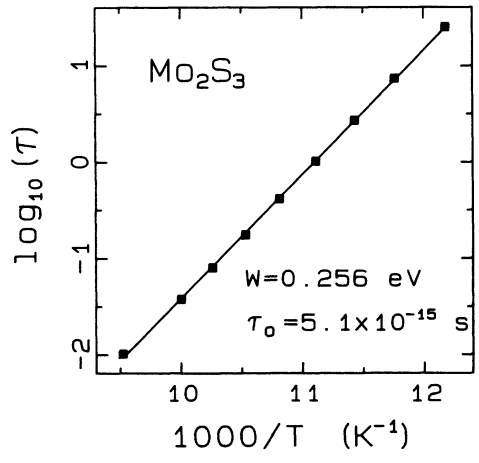

FIG. 9. Time constant of Mo_2S_3 determined from the pulsed-conductivity measurements plotted as a function of $1000/T$. The squares are the measured time constants and the solid line is a least-squares fit to the equation $\tau=\tau_0\exp(W/kT)$.

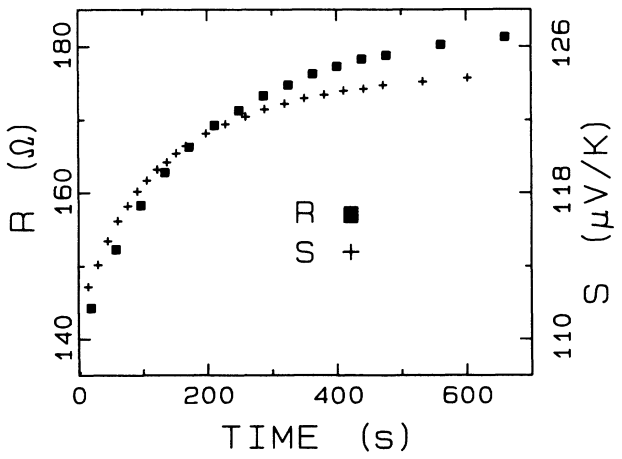

FIG. 10. Time dependence of the thermoelectric power (pluses) and the resistance (squares) of Mo_2S_3 after rapid thermal quenching. The sample temperature was 77 K.

magnitude greater than the thermoelectric voltage, so no corrections for this effect were necessary). While the resistance and thermopower data are similar, the fractional change in the resistance over the period of the measurement is about 19%, while the corresponding change in the thermopower is only 11%.

In Fig. 11 the quantities $\log_{10}[R^{-1}(t)-R^{-1}(\infty)]$ and $\log_{10}[S^{-1}(t)-S^{-1}(\infty)]$ are plotted as a function of time. Since $G \propto R^{-1}$, such a plot should result in a straight line. As can be seen, however, the plot in Fig. 11(a) has an upward curvature with respect to the solid line, which represents a least-squares fit to the data. This curvature is not unexpected, since a temperature gradient was present during the resistance measurements. The gradient results in a distribution of relaxation times, which, it is easy to show, will result in an upward curvature, as is observed.

Despite the nonlinearity of the data, the relaxation times found from the least-squares fits in Fig. 11 should be approximately correct. With this assumption, the relaxation time from the resistance data is 230 s, while that for the thermopower data is 210 s. This suggests that the time dependencies of the thermopower and the conductance have a common origin. The fact that the conductance shows a change of greater magnitude than the thermopower is presumably due to the fact that the thermopower is not simply proportional to the number of carriers.[28]

IV. THE DOUBLE-WELL-POTENTIAL MODEL

At this point let us consider only the temperature region below the lower-temperature phase transition—below 145 K. In this temperature region the conductivity falls, goes through a minimum at 80 K, and then rises again. It is also this temperature region where the time-dependent conductivity and thermoelectric power are observed. Further, the linear dependence of $\log_{10}(\tau)$ on $1/T$ suggests that thermal-activation processes are important. These observations lead us to suggest a double-well-potential model for the carriers, as illustrated in Fig. 12. In this model the carriers can be either in a low-conductivity ground state or in a relatively-high-conductivity metastable state, with a large energy barrier existing between the two wells. The double-well potential shown in Fig. 12 is not necessarily a potential well in real space; it is meant only to represent the existence of two states for the carriers. The presence of the energy barrier between the ground state and the metastable state does not affect the equilibrium distribution of carriers in each state. It does, however, serve to define a transition rate for carriers transferring from one state to the other. If thermally activated hopping over the energy barrier is assumed to be dominant over quantum-mechanical tunneling through the barrier, then the frequency of a successful hopping event, f, can be written as[29]

$$f = f_0 \exp(-W/kT) ,$$

where f_0 is an attempt frequency for barrier crossing and W is the barrier energy. Letting $f^{-1}=\tau$ and $f_0^{-1}=\tau_0$ gives

$$\tau = \tau_0 \exp(W/kT) ,$$

which is just Eq. (2).

A. Temperature dependence of the conductivity

The charge-density temperature dependence, $n(T)$, can be calculated in a straightforward fashion. If the system is in thermal equilibrium, then

$$n_H/n_L = \exp(-E/kT) , \quad (3)$$

where n_H is the carrier density in the high-conductivity

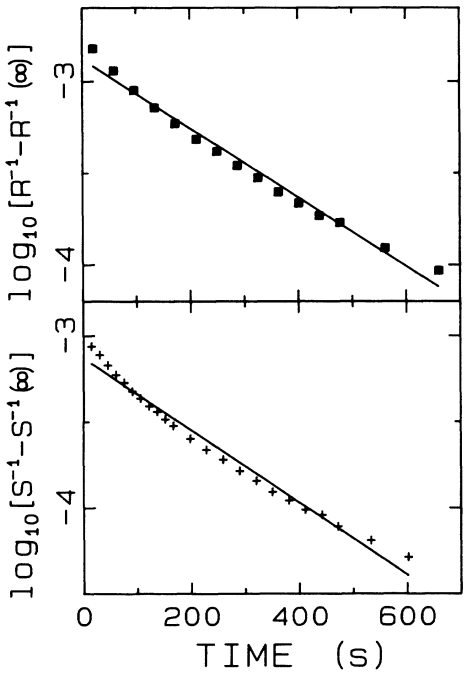

FIG. 11. (a) $\log_{10}[R(t)^{-1}-R(\infty)^{-1}]$ vs time and (b) $\log_{10}[S(t)^{-1}-S(\infty)^{-1}]$ vs time, for Mo_2S_3 after rapid thermal quenching. The symbols are the measured values and the curves are least-squares fits to a straight line.

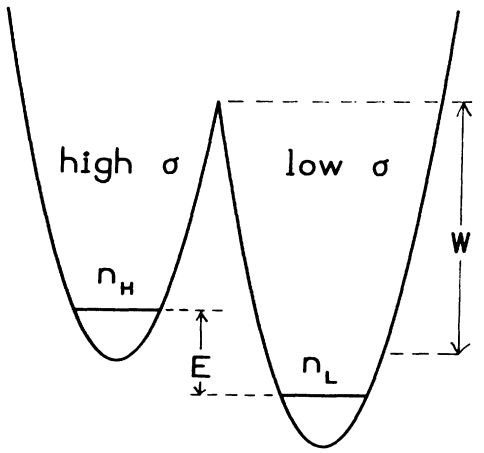

FIG. 12. Double-well-potential model for Mo_2S_3. The left-hand well has n_H highly conducting carriers per unit volume, while the right-hand well has n_L poorly conducting carriers per unit volume.

(metastable) state, n_L is the density of carriers in the low-conductivity (ground) state, and E is the energy difference between the two states. We assume that the total carrier density n_0 is constant, so that $n_H+n_L=n_0$. Then,

$$n_H(T)=\frac{n_0}{1+\exp(E/kT)} \tag{4}$$

and

$$n_L(T)=\frac{n_0}{1+\exp(-E/kT)} . \tag{5}$$

If, for simplicity, the conductivity of carriers in the ground state is taken to be zero, then we find the sample conductivity to be

$$\sigma(T)=\frac{n_0 e^2 \tau_S(T)}{m[1+\exp(E/kT)]} . \tag{6}$$

In order to estimate the temperature dependence of τ_S, the carrier-scattering time, it is observed that at temperatures above 200 K the conductivity exhibits a metalliclike behavior, being approximately proportional to $1/T$. This suggests that τ_S varies as T^{-1}. If this also holds for temperatures below 145 K, then the conductivity can be written as

$$\sigma(T)\propto\frac{1}{T}\frac{1}{1+\exp(E/kT)} . \tag{7}$$

Caution should be taken in placing too much faith in this result, but its only purpose here is to obtain an estimate of the energy difference, E. By comparing Eq. (7) with the resistivity data between 80 and 145 K (Fig. 2), E was estimated to fall in the range $10<E<20$ meV. It is not essential for the development of the model to obtain a precise value for E, but, as will be shown, it is only necessary that E be small in comparison with W.

B. Temperature dependence of the relaxation time

The time-dependent nonequilibrium conductivity observed experimentally can be treated within the framework of this model. The rate of change of the carrier density in the metastable state can be written as

$$\frac{dn_H}{dt}=g(n_H)-r(n_H) , \tag{8}$$

where $g(n_H)$ is the rate at which carriers cross over the barrier from the ground state to the metastable state, and $r(n_H)$ is the rate for the reverse transition. These rates are, in general, dependent on n_H, as $g(n_H)$ must be zero if $n_H=n_0$ and $r(n_H)$ must be zero if $n_H=0$

If only weak carrier-carrier interactions are assumed, then the transition rates are expected to be proportional to the respective carrier densities, so that

$$g(n_H)=n_L/\tau_L=(n_0-n_H)/\tau_L \tag{9}$$

and

$$r(n_H)=n_H/\tau_H , \tag{10}$$

where τ_L is the relaxation time for a carrier initially in the nonconducting state and τ_H is the same for a carrier initially in the conducting state.

Now let us assume that the system is initially disturbed from thermal equilibrium, so that $n_H=n_{H0}+\Delta n_{H0}$, where n_{H0} is the thermal equilibrium value and Δn_{H0} is the initial size of the disturbance. Then, using Eqs. (8)–(10), we have

$$\Delta n_H=n_H-n_{H0}=\Delta n_{H0}\exp(-t/\tau) ,$$

where τ is given by $\tau=\tau_H\tau_L/(\tau_H+\tau_L)$.

Since the conductivity is proportional to the carrier density, and assuming that the conductivity of the ground state is zero, we can write

$$\Delta\sigma(t)=\Delta\sigma_0\exp(-t/\tau) . \tag{11}$$

This equation is the equation used to fit the measured time-dependent sample conductance after the onset of the lower current (see Fig. 8).

In order to calculate $\tau(T)$ from this model, the lifetimes in the two states, τ_H and τ_L, must be defined. This can be done in a straightforward fashion by noting that the barrier energy, shown in Fig. 12, as seen by a carrier in the upper or lower potential well is $W\pm E/2$, so that

$$\tau_H=\tau_{H0}\exp[(W-E/2)/kT]$$

and

$$\tau_L=\tau_{L0}\exp[(W+E/2)/kT] .$$

At equilibrium, $dn_H/dt=0$, which leads to the result

$$\tau_H/\tau_L=\exp(-E/kt) ,$$

which requires $\tau_{H0}=\tau_{L0}=\tau_0$, and gives

$$\tau(T)=\frac{\tau_0\exp(W/kT)}{\exp(E/2kT)+\exp(-E/2kT)} . \tag{12}$$

It is observed that the asymmetry of the double-well potential is responsible for the term in the denominator of Eq. (12), and so Eq. (12) is a good approximation to Eq. (2) only if $E\ll W$. This condition is well satisfied by the values of E and W determined experimentally. As T changes from 80 to 130 K, the denominator changes by a factor of about 1.4, while $\exp(W/kT)$ changes by a factor greater than 10^6.

C. Comparison with experimental results

As we have seen, the double-well-potential model predicts the time-dependent conductivity and time-dependent thermopower in Mo_2S_3. The model also predicts the temperature-dependent conductivity as given in Eq. (6). According to Eq. (6) the conductivity should continue to fall below 80 K, whereas experimentally the conductivity goes through a minimum at 80 K and rises in a metalliclike fashion below that temperature. This behavior is completely consistent with the double-well-potential model. As the temperature is lowered towards 80 K, the relaxation-time constant becomes several minutes, and at 70 K the time constant is expected to be nearly 3 h. Thus, for typical sample cooling rates of 0.25 K/min, the carriers will not remain in thermal equilibri-

um during the measurement. The carriers cannot transfer from the metastable state to the ground state at a rapid enough rate—they become frozen in the metastable state, and the conductivity behavior becomes metalliclike at low temperatures.

As the temperature is lowered, one expects that the transition rate due to quantum-mechanical tunneling will eventually dominate thermally activated hopping. We carried out one experiment at low temperatures to test this hypothesis. The sample was slowly cooled to 4.2 K and its resistance was monitored over a period of several days. The predicted hopping time constant at 4.2 K is 10^{296} yr, so that any increase in the resistance with time would be attributed to quantum-mechanical tunneling of carriers from the high-conductivity state to the low-conductivity state. During this experiment, essentially no change in resistance was observed, suggesting that tunneling is unimportant. (In fact, a small decrease in the resistance, on the order of 0.01%, was observed, but this could have been due to a time-dependent thermal emf.)

At this point we are also able to explain the details of the observed time-dependent conductivity. Referring back to Fig. 6(c), at the onset of the high-current pulse, the conductivity first falls rapidly, goes through a minimum, and then rises until it asymptotically approaches a constant value. The initial fall in the conductivity is due to the heating caused by the current pulse, which leads to an increase in the carrier-scattering rate by phonons. The carrier-hopping time, for the measurements presented here, is much longer than the thermal time constant (believed to be ~ 1 ms). Thus, as the sample heats up the scattering by phonons increases, lowering the conductivity. Then carriers begin transferring from the ground state to the metastable state, so that the conductivity rises, asymptotically approaching the new steady-state value. At the onset of the lower current, the behavior is simply reversed. The sample cools rapidly, thus reducing the scattering by phonons and hence increasing the conductivity. Then the excess carriers slowly transfer from the metastable state to the ground state, giving rise to the exponential time dependence of the conductivity.

V. POSSIBLE ORIGINS OF THE DOUBLE-WELL POTENTIAL

The preceding analysis shows that the double-well-potential model can predict the observed features of the conductivity of Mo_2S_3 below 145 K in considerable detail. The question remains as to the physical mechanism responsible for creating the double-well potential. In this section we outline three possible sources of the double-well potential. These models will also be discussed in a planned second paper dealing with conductivity fluctuations in Mo_2S_3.[30]

A. The carrier-trapping model

Perhaps the simplest physical picture of the electronic properties of Mo_2S_3 is a single-carrier-trapping model, in which the trapping occurs at impurity or other defect sites. Such a model could be appropriate in view of the fact that Mo_2S_3 tends to be metal rich, and also in view of possible contamination by iodine during the crystal-growth process. To be consistent with the experimental results, the defect would obviously have to produce a trapping site (potential-energy minimum) separated from the free-carrier state by a rather large potential-energy barrier. Trapping of the carriers would then remove them from the conduction process. Random thermal excitation of the carriers out of the traps would allow conduction to occur, with the average number of free carriers determining the magnitude of the conductivity.

If the trapping sites were due to the presence of extrinsic defects, one might expect sample-to-sample or growth-batch–to–growth-batch variations in the sample conductivity and/or measured time constants. No such variations were observed in our samples. Further, samples grown with Sn as the transporting agent show the expected temperature-dependent resistivity.[14] Similarly, if the trapping were due to intrinsic defects such as dislocations, one might expect sample-to-sample variations due to differences in sample history. That is, such things as the number of electrical contacts, the type of electrical contacts, and the number of thermal cycles could all play a role in the determination of the conductivity and the measured time constants. However, all samples measured showed the same room-temperature conductivity within experimental error limits ($\pm 20\%$) and the same value of the barrier height within 2%.

Another source of defects might be the electrical contacts themselves, but this is quite likely. We found no evidence of intercalation of the silver-paint chemical components into Mo_2S_3, in that conductivity measurements on samples with contacts that were several months old resulted in the same sample conductivity as when the sample contacts were first attached. Further, it should be noted that some samples were studied using contacts made by pressing between two copper blocks (no silver paint). These samples showed the same phase-transition temperatures and the same low-temperature time constants as samples which had silver-paint contacts.

It is also possible that the presence of iodine in the samples could lead to defects of the sort required. The samples investigated here were all grown with ~ 5 mg/cm^3 of iodine in the growth tube. X-ray-fluorescence measurements showed no traces of iodine at the detection limit of 2 at.%. Further, one would expect sample-to-sample variations in the amount of iodine present, with consequent changes in the conductivity properties. In addition, Alova and Mozurkewicz,[14] in their measurements of internal friction, found a thermally activated internal-friction peak, with barrier height and hopping times similar to ours, but their samples were growth with Sn, not I, as the transporting agent.

B. The acoustic-polaron model

The concept of the polaron was introduced by Landau[31] as a process whereby an electron (or hole) can interact with a deformable lattice. Through this interaction the charge carrier can become localized in the lattice, or "self-trapped." A great deal of attention has been given to this problem in the literature and only a brief

survey of the properties of the acoustic-mode polaron will be given here. The result important to the discussion here is that the acoustic-polaron model can give rise to a double-well potential of the form necessary to explain the observed electronic behavior of Mo_2S_3.

The various polaron models assume that a charge carrier in a deformable medium can interact with the vibrations of the medium via long-range Coulomb forces (optical phonons) or the short-range deformation potential produced by the acoustic phonons of the medium. The self-trapped states formed due to the long-range Coulomb interaction are referred to as dielectric (or large) polarons, while those formed from the acoustic-vibrational modes are called acoustic (or small) polarons. Qualitatively, the difference between these two types of self-trapped states is in the behavior of their effective masses (carrier-plus-lattice deformation) as the degree of coupling between the carrier and the lattice increases. The dielectric polaron effective mass increases continuously as the interaction strength increases. In contrast, the effective mass of the acoustic polaron undergoes a discontinuous jump as the coupling is increased. This change in effective mass may be as large as several orders of magnitude. Where this occurs, the carrier becomes so "heavy" that it is essentially frozen in the lattice. It is the acoustic polaron which will be discussed here.

Holstein,[32] in his pioneering work on the small polaron, used the deformation-potential–carrier interaction to produce a self-trapped state in a one-dimensional molecular-crystal model. Of more interest here, though, is the work of Toyozawa[33] in three dimensions. Toyozawa assumed a uniform dilation of the lattice inside a sphere of radius R, with the deformation energy being proportional to the size of the dilation. He showed that a bound state (self-trapped state) will be produced if the dilation is large enough. In the case of a discrete lattice, he was able to show that, along with the acoustic-polaron ground state, a metastable state is also produced in which the charge carrier is delocalized, or untrapped, with an adiabatic potential barrier separating the trapped and delocalized states. Toyozawa speculated that if this barrier energy is large enough, very-long-lived free-carrier states could be produced.

Small-polaron formation is also discussed by Mott and Davis[34] and Mott and Stoneham.[35] Using a simplified version of the lattice-carrier interaction producing the free and self-trapped states, they represent the degree of the lattice distortion by a configurational coordinate q. Neglecting the kinetic energy of the carrier, they find the carrier-plus-lattice energy W to be

$$W = Aq^2/2, \quad q < q_c$$
$$W = Aq^2/2 - E_d(q - q_c), \quad q > q_c \ . \tag{13}$$

The constant A in the above equations corresponds to an elastic constant of the lattice, while q_c is the minimum lattice distortion required to produce a bound state. The terms involving q^2 represent the increase in potential energy due to the lattice distortion and the term linear in q is the energy reduction resulting from the formation of the bound state, consistent with Toyozawa's model. Plotting W as a function of q gives an interesting picture of the system, as shown in Fig. 13. The center curve represents the sum of the linear and quadratic terms in Eq. (13). W_B and E_b are the barrier energy and small-polaron binding energy, respectively. This figure is qualitatively identical with the phenomenological double-well potential used to describe Mo_2S_3. Using typical values for the various parameters in the acoustic-polaron model, one can calculate values of $W_B = 0.5$ eV and $E_b = 33$ meV. These values are similar to the measured values of 0.25 eV and ~ 15 meV, respectively.

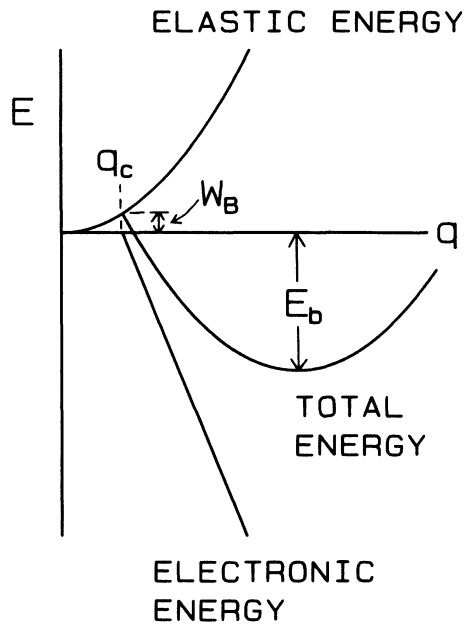

FIG. 13. Carrier energy as a function of configurational coordinate in the acoustic-polaron model. q_c is the minimum lattice distortion required to produce a bound state. The curves indicating the lattice energy, the electron bound-state energy, and the total energy are labeled.

C. The charge-density-wave model

In view of its quasi-one-dimensional character and the presence of phase transitions, it would seem reasonable to assume that Mo_2S_3 is a charge-density-wave system similar to $NbSe_3$ or TaS_3. This would appear especially likely since Deblieck *et al.*[11] found both commensurate and incommensurate structural distortions to be associated with the phase transitions and, further, that the phase transitions result in a loss of Fermi surface. Such properties appear to be endemic to charge-density-wave systems.

In addition to the anomalies in the resistivity found at the charge-density-wave transition temperatures, $NbSe_3$ and TaS_3 exhibit nonlinear conductivity when the electric field, E, is greater than a well-defined critical threshold value, E_{cr}. The nonlinear conductivity in these compounds is believed to be caused by the electric field depinning the approximately rigid charge-density-wave structure, enabling it to participate in the conduction process. Related to this nonlinear conductivity is the occurrence

of an unusually large amount of excess current noise for $E > E_c$, where E_c is the critical value of the electric field in the sample below which no excess noise is found.[3] The electrical noise generally has a broadband component in the low-frequency range and narrow-band components in the MHz range. The narrow-band noise appears to be associated with the regular motion of the charge-density maxima past the electrical contacts, but the origin of the broadband noise has not yet been firmly established. It should also be noted that the critical fields E_{cr} and E_c are generally not equal for a given compound (although they are usually similar in magnitude) and are generally temperature dependent below the transition temperature.

No nonlinear conductivity was observed in Mo_2S_3 using either dc currents or pulsed currents up to 10 V/cm. This implies that if a charge-density wave forms in Mo_2S_3, it is very strongly pinned to the lattice or to defects. It appears as if $E_{cr} \sim \infty$. However, broadband electrical noise is observed in Mo_2S_3 for temperatures below 200 K. The results of these measurements will be presented in a planned subsequent paper,[30] but we summarize the main results here. The noise first appears as the temperature is lowered below 200 K. The critical electric field for the noise, E_c, appears to be zero, and the magnitude of the noise power is proportional to I^2. The temperature dependence and frequency dependence of the broadband noise is quite consistent with the predictions of the double-well-potential model. (In the double-well-potential model the electrical noise arises because of the thermal fluctuations of the carrier densities in the two wells of the potential.) These results are quite different from the corresponding observations in the well-known charge-density-wave conductors.

In view of these results, we conclude that if Mo_2S_3 is a charge-density-wave system, it must be quite different than $NbSe_3$ or TaS_3.

VI. DISCUSSION

Three models which can possibly explain the electronic properties of Mo_2S_3 have just been presented. The defect-trapping model and the acoustic-polaron model are both single-carrier models, in that no cooperative motion of the carriers is expected. The charge-density-wave model, however, involves a condensation of the carriers into a spatially periodic charge-density wave in which cooperative motion of the carriers is possible (as in depinning). While we have not presented our electrical-noise data on Mo_2S_3, one important point should be made: The frequency dependence of the electrical noise is consistent with the prediction of the double-well-potential model, and the magnitude of the noise power is quite large. Our Hall-effect measurements, and those discussed by Rastogi,[13] indicate that Mo_2S_3 has greater than 10^{20} holes/cm^3. Using this carrier concentration, the magnitude of the noise power predicted by the double-well-potential model is more than 3 orders of magnitude smaller than the observed noise power. For the double-well-potential model to predict the correct noise-power magnitude, either the carrier concentration must be less than 10^{17} cm^{-3}, or a cooperative motion of the carriers must occur. This result strongly suggests that the motion of the carriers is cooperative, and so favors the charge-density-wave model over either of the single-carrier models. It is not easy to see how the defect-trapping model or the acoustic-polaron model can result in cooperative motion of the carriers. Furthermore, the defect-trapping model cannot give rise to the observed phase transitions.

In spite of the difficulty with the carrier concentration the acoustic-polaron model does have two points in its favor. It can certainly give rise to a double-well potential of the type needed to explain our experimental results. It also holds some promise in its ability to explain the presence of the phase transitions. Toyazawa[33] has shown that the effective mass of the carriers can change discontinuously as a function of the carrier-lattice coupling. This could, of course, result in the conductivity behavior observed experimentally at the phase transitions. However, to date no convincing experimental evidence exists for an acoustic-polaron-driven phase transition in any system.

The charge-density-wave model of conduction in Mo_2S_3 has a natural appeal. Mo_2S_3 is a linear-chain-structure compound that shows phase transitions apparently similar in nature to the phase transitions observed in the known charge-density-wave systems $NbSe_3$ and TaS_3. $NbSe_3$ and TaS_3 are also linear-chain-structure compounds. Furthermore, the charge-density-wave model can result in a large excess noise magnitude even when the sample has a large carrier concentration. The large noise magnitude arises because a whole charge-density-wave segment can break loose and contribute to the conductivity. The effective charge of such a segment might be 10^4e. In this case, perhaps a realistic physical picture would be the charge-density-wave segment being pinned by solitonlike kinks and antikinks. The destruction of a kink (perhaps by thermal excitation) would allow the segment to conduct. Thus the phenomenological double-well potential would be associated with the kinks and antikinks, rather than with the individual free carriers. It has, however, not been shown that kink formation can lead to a double-well potential of the kind required by experiment. Clearly, more theoretical work needs to be done.[36,37]

At this point it also seems difficult to reconcile the charge-density-wave model with all of the experimental results. Experimentally, the critical electric field for generation of excess noise seems to be zero and the critical field for nonlinear conductivity seems to be infinite, or at least larger than can be experimentally achieved. None of the existing theories of charge-density-wave formation predict this kind of behavior.

Thus, while it is not possible to rule out a charge-density-wave model for Mo_2S_3, it seems that existing models are inadequate to explain the experimental results presented here.

ACKNOWLEDGMENTS

We would like to thank T. Holstein for suggesting that acoustic polarons may play a role in the properties of Mo_2S_3, J. R. Hardy and R. J. Hardy for helpful discussions, and James McCarthy for his efforts in making the Hall-effect measurements. We would particularly like to thank E. A. Pearlstein for his constant interest in this problem and for innumerable helpful discussions.

[1]P. Monceau, N. P. Ong, A. M. Portis, A. Meerschant, and J. Rouxel, Phys. Rev. Lett. **37**, 602 (1976).
[2]T. Sambongi, K. Tsutsumi, Y. Shiozaki, M. Yamanoto, K. Yamaya, and Y. Abe, Solid State Commun. **22**, 729 (1977).
[3]R. M. Fleming and C. C. Grimes, Phys. Rev. Lett. **42**, 1423 (1979).
[4]A. H. Thompson, A. Zettl, and G. Grüner, Phys. Rev. Lett. **47**, 64 (1981).
[5]N. P. Ong and P. Monceau, Phys. Rev. B **16**, 3443 (1977).
[6]G. Grüner, Comments Solid State Phys. **10**, 183 (1983).
[7]F. Jellinek, Nature (London) **192**, 1065 (1961).
[8]F. Kadjik, R. Huisman, and F. Jellinek, Acta Crystallogr. Sect. B **24**, 1102 (1968).
[9]R. DeJonge, T. Popma, G. Wiegers, and F. Jellinek, J. Solid State Chem. **2**, 188 (1970).
[10]A. K. Rastogi and R. K. Ray, Bull. Mater. Sci. **3**, 341 (1981).
[11]R. Deblieck, G. A. Wiegers, K. D. Bonsema, D. van Dyck, G. van Tendeloo, J. van Landuyt, and S. Amelinckx, Phys. Status Solidi A **77**, 249 (1983).
[12]M. H. Rashid, D. J. Sellmyer, V. Katkanant, and R. D. Kirby, Solid State Commun. **43**, 675 (1982).
[13]A. K. Rastogi, Philos. Mag. B **52**, 909 (1985).
[14]Alova and G. Mozurkewich, J. Phys. (Paris) Colloq. **46**, C10-685 (1985).
[15]J. A. Wilson, F. J. DiSalvo, and S. Mahajan, Adv. Phys. **24**, 117 (1975).
[16]F. J. DiSalvo and J. Waszczak, Phys. Rev. B **17**, 3801 (1978).
[17]F. J. DiSalvo, J. A. Wilson, B. G. Bagley, and J. V. Waszczak, Phys. Rev. B **12**, 2280 (1975).
[18]J. A. Wilson and S. Mahajan, Phys. Status Solidi B **81**, 11 (1978).
[19]G. Grüner, Physica **80**, 1 (1983), and references therein.
[20]P. Monceau, J. Richard, and M. Renard, Phys. Rev. Lett. **45**, 43 (1980).
[21]M. Weger, G. Grüner, and W. G. Clark, Solid State Commun. **35**, 243 (1980).
[22]N. P. Ong and C. M. Gould, Solid State Commun. **37**, 25 (1981).
[23]G. Grüner, A. Zettl, W. G. Clark, and A. H. Thompson, Phys. Rev. B **23**, 6813 (1981).
[24]R. Peierls, *Quantum Theory of Solids* (Clarendon, Oxford, 1975).
[25]H. Fröhlich, Proc. R. Soc. London, Ser. A **223**, 296 (1954).
[26]G. Krabbes, H. Opperman, and J. Henke, Z. Anorg. Allg. Chem. **470**, 7 (1980).
[27]Y. Suzuki, T. Uchida, M. Wakihara, and M. Taniguchi, Mater. Res. Bull. **16**, 1085 (1981).
[28]F. J. Blatt, P. A. Schroeder, C. L. Foiles, and D. Grieg, *Thermoelectric Power of Metals* (Plenum, New York, 1976).
[29]See, for example, M. Ali Omar, *Elementary Solid State Physics* (Addison-Wesley, Reading, Mass., 1975), pp. 539ff.
[30]R. L. Fagerquist, R. D. Kirby, and E. A. Pearlstein (unpublished).
[31]L. Landau, Phys. Z. Sowjetunion **3**, 664 (1933).
[32]T. Holstein, Ann. Phys. (N.Y.) **8**, 325 (1959).
[33]Y. Toyozawa, Prog. Theor. Phys. **26**, 29 (1961).
[34]N. F. Mott and E. A. Davis, *Electronic Properties of Non-Crystalline Materials* (Clarendon, Oxford, 1979).
[35]N. F. Mott and A. M. Stoneham, J. Phys. C **10**, 3391 (1977).
[36]J. Richard, P. Monceau, M. Papoular, and M. Renard, J. Phys. C **15**, 7157 (1982).
[37]M. Papoular, Phys. Rev. B **25**, 7856 (1982).